



^{10}Be in late deglacial climate simulated by ECHAM5-HAM – Part 1: Climatological influences on ^{10}Be deposition

U. Heikkilä¹, S. J. Phipps², and A. M. Smith¹

¹Institute for Environmental Research, Australian Nuclear Science and Technology Organisation (ANSTO), Lucas Heights, NSW, Australia

²ARC Centre of Excellence for Climate System Science and Climate Change Research Centre, University of New South Wales, Sydney, Australia

Correspondence to: U. Heikkilä (ulla.heikkilae@eawag.ch)

Received: 12 June 2013 – Published in Clim. Past Discuss.: 2 July 2013

Revised: 25 October 2013 – Accepted: 1 November 2013 – Published: 25 November 2013

Abstract. Reconstruction of solar irradiance has only been possible for the Holocene so far. During the last deglaciation, two solar proxies (^{10}Be and ^{14}C) deviate strongly, both of them being influenced by climatic changes in a different way. This work addresses the climate influence on ^{10}Be deposition by means of ECHAM5-HAM atmospheric aerosol–climate model simulations, forced by sea surface temperatures and sea ice extent created by the CSIRO Mk3L coupled climate system model. Three time slice simulations were performed during the last deglaciation: 10 000 BP (“10k”), 11 000 BP (“11k”) and 12 000 BP (“12k”), each 30 yr long. The same, theoretical, ^{10}Be production rate was used in each simulation to isolate the impact of climate on ^{10}Be deposition. The changes are found to follow roughly the reduction in the greenhouse gas concentrations within the simulations. The 10k and 11k simulations produce a surface cooling which is symmetrically amplified in the 12k simulation. The precipitation rate is only slightly reduced at high latitudes, but there is a northward shift in the polar jet in the Northern Hemisphere, and the stratospheric westerly winds are significantly weakened. These changes occur where the sea ice change is largest in the deglaciation simulations. This leads to a longer residence time of ^{10}Be in the stratosphere by 30 (10k and 11k) to 80 (12k) days, increasing the atmospheric concentrations (25–30 % in 10k and 11k and 100 % in 12k). Furthermore the shift of westerlies in the troposphere leads to an increase of tropospheric ^{10}Be concentrations, especially at high latitudes. The contribution of dry deposition generally increases, but decreases where sea ice changes are largest. In total, the ^{10}Be deposition rate changes by no more

than 20 % at mid- to high latitudes, but by up to 50 % in the tropics. We conclude that on “long” time scales (a year to a few years), climatic influences on ^{10}Be deposition remain small (less than 50 %) even though atmospheric concentrations can vary significantly. Averaged over a longer period, all ^{10}Be produced has to be deposited by mass conservation. This dominates over any climatic influences on ^{10}Be deposition. Snow concentrations, however, do not follow mass conservation and can potentially be impacted more by climate due to precipitation changes. Quantifying the impact of deglacial climate modulation on ^{10}Be in terms of preserving the solar signal locally is analysed in an accompanying paper (Heikkilä et al., ^{10}Be in late deglacial climate simulated by ECHAM5-HAM – Part 2: Isolating the solar signal from ^{10}Be deposition).

1 Introduction

Cosmogenic radionuclides, such as ^{10}Be and ^{14}C , are commonly used proxies for solar activity. Their production rate in the atmosphere responds to changes in cosmic ray intensity, which again is modulated by solar activity and the strength of the geomagnetic field. Their transport from the source to natural archives is subject to climatological modulation: atmospheric circulation and precipitation in the case of ^{10}Be and reservoir exchange times in the case of ^{14}C . Comparison of both radionuclides allows for the separation of the common production, or solar, signal from the climate modulation. Recent results show that during the Holocene the

climate impact remains relatively small and that the solar signal can be retrieved (e.g. Roth and Joos, 2013; Steinhilber et al., 2012). However, extending the solar forcing function to the last deglaciation becomes challenging, as large discrepancies arise between ¹⁴C and ¹⁰Be (e.g. Muscheler et al., 2004). The reason for these differences has to be understood before the solar forcing function can reliably be extended to this period.

In order to address the sensitivity of ¹⁰Be deposition onto polar ice sheets to climate changes, we perform time slice simulations within the deglacial climate at three different stages: 12 000 BP (years before 1950 CE), 11 000 BP and 10 000 BP. A preindustrial control simulation is also performed for comparison. These simulations are referred to as “ctrl”, “12k”, “11k” and “10k” throughout the manuscript. The model employed is the ECHAM5-HAM aerosol–climate model. This incorporates the aerosol module HAM, which describes aerosol emission, physical and chemical as well as deposition processes. This model only describes the atmosphere and hence requires the sea surface temperatures and sea ice cover to be prescribed. In this study these variables were generated using the CSIRO Mk3L climate system model, which comprises components describing the atmosphere, land, sea ice and ocean (Phipps et al., 2011, 2012). ECHAM5-HAM resolves aerosol processes explicitly. This is important in order to obtain a realistic picture of aerosol deposition and its climate modulation, but at the same time it increases the runtime of the model. Such a time-slice approach focusing on periods of special interest, such as the Last Glacial Maximum or the mid-Holocene, is commonly used in model intercomparison experiments (e.g. Braconnot et al., 2012), or when addressing questions such as atmospheric particle transport under a changing climate (e.g. Krinner et al., 2010; Mahowald et al., 2006).

The focus of this study is to investigate the impact of the deglacial climate on ¹⁰Be deposition. The reconstructing of the solar signal from the ¹⁰Be deposition rate during this period is addressed in an accompanying paper (Heikkilä et al., 2013b). In order to be able to distinguish the imprint of climate only, and also because the actual solar activity and therefore the ¹⁰Be production rate are unknown, we use the same (theoretical) production rate in all simulations. This means that even if the model climate in each time slice simulation is quite different, the global mean ¹⁰Be deposition rate will be equal due to mass conservation. Because of this a direct comparison with measured ¹⁰Be concentrations is not possible. In terms of climate these time slice simulations produce typical climatic conditions given the boundary conditions determined by greenhouse gas concentrations (GHGs), orbital parameters and aerosol load. The internal climate variability produced by the model will be representative in a statistical sense under these boundary conditions, although the actual timing and magnitude of individual weather events will not be reproduced.

Table 1. Global mean greenhouse gas concentrations (used as forcing for the simulations), surface temperature and precipitation rate (model results from the simulations).

	ctrl	10k	11k	12k
Greenhouse gas concentrations				
CH ₄ (ppb)	760.0	702.9	701.3	479.3
CO ₂ (ppm)	280.0	265.0	263.0	240.6
N ₂ O (ppb)	270.0	269.9	267.8	242.3
Surface temperature (°C)	15.2	14.4	14.1	12.5
Precipitation rate (mm day ⁻¹)	3.06	2.98	2.96	2.85

Comparison of ¹⁰Be and ¹⁴C during the Younger Dryas has previously been used to detect changes in North Atlantic deep-water formation and the carbon cycle (Muscheler et al., 2000, 2004); however, both ¹⁰Be and ¹⁴C are influenced differently by changes in climatic conditions, which hampers the detection of the common solar signal. A recent study by Roth and Joos (2013), employing a three-dimensional dynamical carbon cycle model, showed that climate-related changes in the carbon cycle lead to significant deviations from previous estimates of ¹⁴C production rate in the early Holocene. To the best of our knowledge, this is the first model study to address ¹⁰Be deposition changes due to climate changes beyond the Holocene.

2 Description of the simulations

Boundary conditions for the ECHAM5-HAM simulations were obtained from simulations of the pre-industrial ctrl, 10k, 11k and 12k climates, conducted using the CSIRO Mk3L climate system model. The model was integrated for 5000 yr in each case to let the system reach thermal equilibrium, and the last 35 yr were then used to provide boundary conditions for the ECHAM5-HAM simulations of the atmosphere. For each time slice simulation, the CSIRO Mk3L simulations used constant orbital parameters and GHGs (obtained from Liu et al., 2009; see Table 1). Land ice extents were prescribed according to ICE-5G reconstruction v1.2 (Peltier, 2004). No changes were made to the global sea level or to the positions of the coastlines.

The ECHAM5-HAM atmospheric model used sea surface temperatures (SST) and sea ice cover generated by the CSIRO Mk3L model as ocean boundary conditions. The GHGs, orbital parameters, orography and land sea mask were set to the same values as in the CSIRO Mk3L simulations. The SSTs and sea ice were updated monthly. Aerosol load was set to preindustrial values for the simulations and was taken from the AEROCOM aerosol model-intercomparison experiment B, available at <http://nansen.ipsl.jussieu.fr/AEROCOM>. The ECHAM5-HAM model was run for 35 yr, of which the first 5 yr were used to spin up the model and discarded. The following 30 yr were used for the

analysis. The horizontal resolution used was the T42 spectral resolution, corresponding to ca. 2.8 degrees or ca. 300 km. The model top was at ca. 30 km, including 31 vertical levels. The model output was analysed monthly. In order to analyse the atmospheric transport path of ¹⁰Be from source to archive, the source regions of ¹⁰Be were divided into 6 compartments: polar, mid-latitude and tropical in both the stratosphere and the troposphere, following Heikkilä et al. (2009) and Heikkilä and Smith (2012). ¹⁰Be produced in these source regions was treated as a separate tracer, and therefore the exact location and timing of deposition could be followed. Scavenging parameters were adjusted to allow for a more realistic particle transport towards the poles, following Bourgeois and Bey (2011).

The ¹⁰Be production rate on the monthly scale was constructed using a low-frequency solar activity parameter Φ based on a reconstruction of the ¹⁴C production rate, and a modern 11-year cycle was added on top. This leads to a ¹⁰Be production rate which is ca. 70 % larger than the known production rate during the last ca. 30 yr (see e.g. Heikkilä and Smith, 2012).

3 Results

3.1 Global means and budgets

Table 1 summarises the global mean temperatures and precipitation rates over each 30 yr period. It is clear from the results that the global mean temperature closely follows the GHGs. The GHGs during 10k and 11k are fairly similar, leading to a cooling of ca. 1 degree from ctrl. The 12k simulation is cooler, 2.7 °C degrees relative to ctrl, due to a larger reduction in the GHGs. These differences are somewhat larger than the 0.6 °C global cooling during the Younger Dryas (12.9 to 11.7 ka BP) reported by Shakun and Carlson (2010). An explicit comparison is hard because the model simulations present two 30 yr snapshots during this period. Shakun and Carlson (2010) analysed all available proxy data worldwide, but large areas, especially oceans, are still uncovered. Because of this their global mean change would be milder if ocean temperatures were given more weight. However, the model simulations presented here have been fully equilibrated, and hence the magnitude of the cooling might exceed the transient response of the climate system.

The precipitation rate varies less between the simulations; however, a linear response to cooling, albeit a weak one, is evident (Fig. 1). Table 2 summarises the global mean ¹⁰Be budgets over each 30 yr period. The ctrl simulation produces results consistent with other model studies for the present-day climate: ca. 2/3 of ¹⁰Be is produced in the stratosphere, and the residence time is of the order of one year in the stratosphere and ca. three weeks in the troposphere (e.g. Heikkilä and Smith, 2012; Koch et al., 2006; Land and Fichter, 2003). The total content of ¹⁰Be in the stratosphere

Table 2. Global mean budgets of ¹⁰Be.

	ctrl	10k	11k	12k
Fraction of production in stratosphere (%)	69	70	70	71
Wet to total deposition (%)	88	88	88	87
Residence time stratosphere (d)	358	386	390	432
Residence time troposphere (d)	22	24	23	25
Content stratosphere (g)	58	63	64	71
Content troposphere (g)	5.2	5.4	5.5	5.7

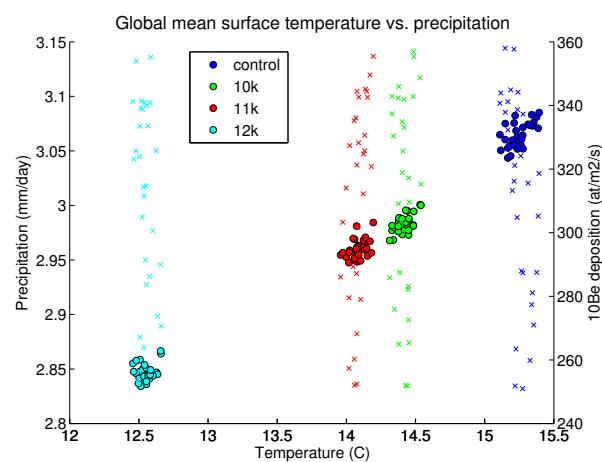


Fig. 1. Simulated global and annual mean precipitation (circles) response to surface temperature change between the simulations. Simulated global and annual mean ¹⁰Be deposition (crosses) response to temperature change. Each marker presents an individual year.

and the troposphere in these simulations is slightly larger than modern values due to the higher production rate.

During the deglaciation the stratospheric fraction of production is slightly increased (1–2 %) due to a lower tropopause height. Again, this change is larger during 12k than 10k and 11k. Moreover, the fraction of wet to total deposition is decreased to 87–88 % in all simulations, which is a reduction relative to the typical simulated present-day value of 91–92 % produced by this model (Heikkilä et al., 2009). The stratospheric and tropospheric residence times are both increased (from 358 to 386–432 days in the stratosphere, from 22 to 23–25 days in the troposphere), leading to higher atmospheric ¹⁰Be content by 22 % in the stratosphere and 10 % in the troposphere; see Table 2. This is likely to be due to circulation changes which will be discussed in the following section.

3.2 Changes in atmospheric circulation

We first investigate the general state of climate in the deglaciation simulations compared with the control climate. Figure 2 shows the zonal mean temperature change relative to ctrl in all simulations. The 10k and 11k simulations show a moderate cooling (1–2 °C) in the tropical upper troposphere

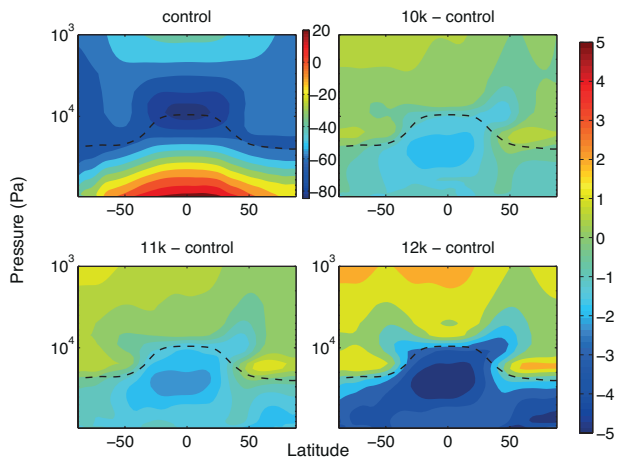


Fig. 2. Top left: zonal mean temperature in the control simulation ($^{\circ}\text{C}$). The remaining: difference from control ($^{\circ}\text{C}$). The zonal mean tropopause height in the control simulation is indicated with the black dashed line.

and a warming ($1\text{--}2^{\circ}\text{C}$) in the stratosphere. The cooling is slightly increased in the 11k simulation, including a cooler region in the northern high-latitude lower levels. This pattern is intensified in the 12k results, with the $50\text{--}90^{\circ}\text{N}$ lower level cooling becoming stronger. A surface cooling and stratospheric warming in response to reduced atmospheric GHGs is consistent with the nature of the observed response to increased GHGs during the 20th century (Trenberth et al., 2007). Zonal mean westerly winds (Fig. 3) show a similar response: a slight weakening (ca. 2 m s^{-1}) of the Southern Hemisphere (SH) mid-latitude and Northern Hemisphere (NH) low-latitude stratospheric winds and a slight intensification (ca. 1 m s^{-1}) in the troposphere (10k and 11k). In the 12k results, again, these changes are intensified. The NH polar jet is shifted by ca. 5° towards the north. A similar shift, although weaker, is observed in the SH mid-latitude jet. The weakening of the stratospheric winds leads to a slower circulation and hence less efficient particle transport, causing the stratospheric residence time of ¹⁰Be to increase by up to ca. 80 days (Table 1).

The shift found in the NH tropospheric westerlies can possibly be connected to the position of storm tracks and therefore to precipitation patterns. However, no such shift is obvious in the precipitation rate (Fig. 4), nor in the sea level pressure (not shown). There is a general decrease (up to 50 %) in the simulated precipitation rate in the mid- and high latitudes (both NH and SH), in agreement with the cooling caused by the lower GHG concentrations (see Fig. 1). At low latitudes, however, there is an increase in precipitation of up to 50 %, mostly in dry areas (Sahara, west of the South American and African continents). In order to study the intensity of internal climate variability we performed an empirical orthogonal functions (EOF) analysis for the sea level pressure. The first EOF of the sea level pressure (SLP, associated with the North

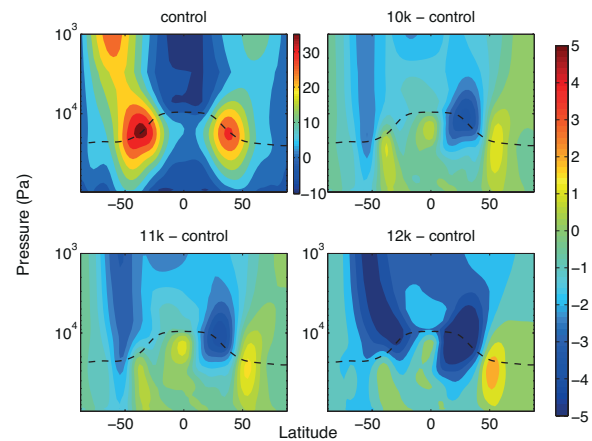


Fig. 3. Top left: Zonal wind in the control simulation (m s^{-1}). The remaining: Difference from control (m s^{-1}). The zonal mean tropopause height in the control simulation is indicated with the black dashed line.

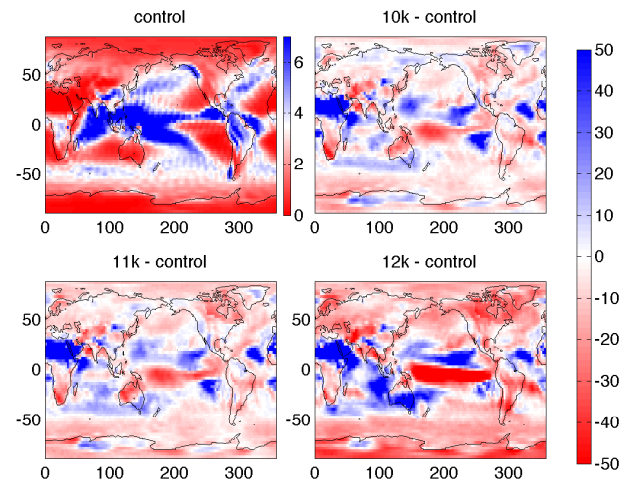


Fig. 4. Top left: Precipitation rate in the control simulation (mm day^{-1}). The remaining: difference from control (%).

Atlantic Oscillation (NAO) in the North Atlantic sector and the Southern Annular Mode (SAM) south of 20° in the SH, Fig. 5) does not exhibit significantly larger variability in the deglaciation simulations than in the control, suggesting that the internal climate variability described by these modes did not change significantly.

The differences between the simulations seem fairly symmetrical except for the shift of the zonal wind in the NH troposphere poleward of 50° . The reason for this asymmetry might be the larger sea ice content in the deglaciation simulations, especially in the NH (Fig. 6). Sea ice conditions influence atmospheric circulation patterns, such as sea level pressure, strength of the westerlies and position of the storm tracks, in the northern mid- and low latitudes and even globally via teleconnections affecting large-scale circulation patterns such as ENSO (e.g. Alexander et al., 2004; Blüthgen

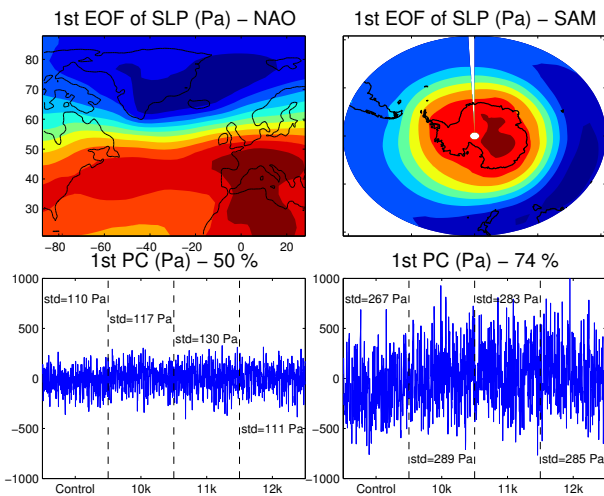


Fig. 5. Empirical orthogonal function (EOF) analysis of sea level pressure for the North Atlantic region (North Atlantic Oscillation, NAO) and the Southern Hemisphere latitudes 20° S–90° S (Southern Annular Mode, SAM). The top subplots show the first EOF of the sea level pressure (SLP, in Pa), and the bottom subplots the first principal component (PC, in Pa) and the variability it explains for the respective areas. The standard deviation (“std”) is shown for each 30 yr period.

et al., 2012; Budikova, 2009; Screen and Simmonds, 2010). However, we find a decrease in geopotential height at the surface, where the sea ice increase is largest both in the NH and the SH, although the anomaly is visible at 500 hPa only in the NH. Thus the 1000–500 hPa thickness is reduced in the deglaciation simulations due to increased sea ice. The reduction is largest near the Hudson Bay area, where sea ice differences are the most pronounced (up to 30 %). This is consistent with Overland and Wang (2010), who found the thickness to increase due to sea ice loss in the Arctic. Furthermore, a shift in the tropopause height is seen at 35° N. This suggests that the anomalous NH temperature, shift in the westerlies and longer atmospheric residence time of ¹⁰Be result from the increased sea ice in the deglaciation simulations.

3.3 Circulation influence on atmospheric distribution of ¹⁰Be

The changes found in climatic conditions of the deglaciation simulations, the weakening of the stratospheric jets, the northward shift in the westerlies and the changes in tropopause height all have the potential to affect particle transport and deposition and hence ¹⁰Be. In the following we investigate the modelled changes in ¹⁰Be between the deglaciation simulations and the control climate. Firstly we investigate whether the general relationship between GHGs, surface temperature and precipitation rate could be used to predict the ¹⁰Be deposition under different climatic conditions. In addition to temperature and precipitation, Fig. 1

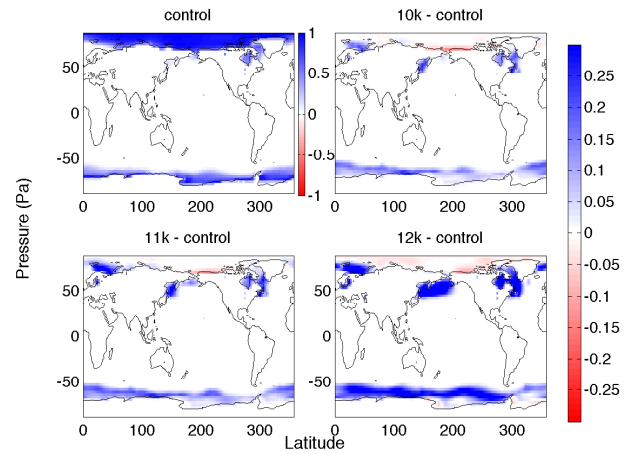


Fig. 6. Fractional sea ice cover in the deglaciation simulations as prescribed by the CSIRO Mk3L model (fraction): top left: control simulation and the remaining: difference from control (fraction).

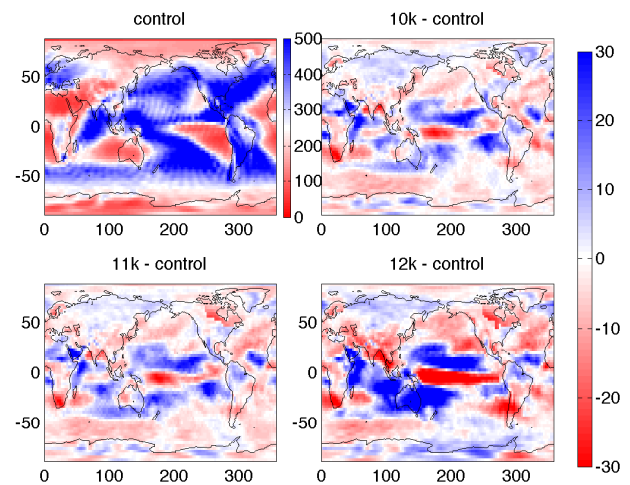


Fig. 7. Top left: ¹⁰Be deposition in the control simulation (atoms m⁻² s⁻¹). The remaining: difference from control (%).

shows the global and annual mean ¹⁰Be deposition flux (crosses) as a function of mean surface temperature for each year of each simulation. No relationship between global mean temperature and ¹⁰Be deposition is obvious because the amplitude of the 11 yr cycle dominates the changes in temperature or precipitation rate. If averaged over the entire 30 yr period, the ¹⁰Be deposition change is zero, as determined by the fact that the production rate is the same. Hence, a simple linear relationship between mean climate and ¹⁰Be deposition cannot be assumed.

Figure 7 illustrates the mean change in ¹⁰Be deposition flux. Because the production rate of ¹⁰Be was the same in all simulations, the global mean change equals zero. ¹⁰Be deposition is not significantly changed at mid- to high latitudes in the 10k and 11k simulations. It is increased by up to 10 % in the NH over Siberia and Greenland, with the exception of

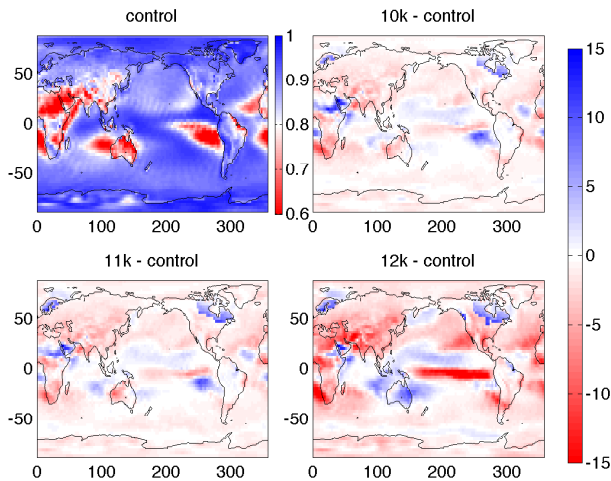


Fig. 8. Top left: wet fraction in the control simulation (i.e. wet deposition divided by total deposition of ^{10}Be (–)). The remaining: difference from control (%).

Scandinavia and the Hudson Bay area (10 to 30%), where changes in sea ice extent are largest. In the SH the ^{10}Be deposition is decreased by up to 20% over the Southern Ocean but generally increased over Antarctica (up to ca. 10%). The change in deposition is larger (> 30%) in the tropical region and its sign varies. Then the difference in deposition in the 12k simulation is similarly distributed but more pronounced than in the 10k and 11k simulations, especially at low latitudes. However, the simulated change at 12k becomes negative over North America, whereas it is slightly positive at 10k and 11k. Over Greenland the deposition increases less at 12k than at 10k or 11k.

The spatial variability of ^{10}Be deposition follows precipitation variability, as Figs. 4 and 7 also show. It is an interplay of precipitation rate and atmospheric concentrations of ^{10}Be . Due to the higher ^{10}Be concentrations in the stratosphere, the location of the stratosphere–troposphere exchange dominates the spatial variability. The maximum in ^{10}Be deposition is found in the mid-latitudes (30–50° N and S), where the precipitation rate is high and the stratosphere–troposphere exchange is also strongest. There is a secondary maximum in the tropics due to the maximum precipitation rate; however, the ^{10}Be air concentrations are low due to the convective uplifting of air from the surface, where ^{10}Be production is minimal. The temporal variability of ^{10}Be deposition has been studied in detail by Heikkilä and Smith (2013a). They show that ^{10}Be deposition strongly correlates with precipitation rate on short time scales (monthly). On annual time scales the correlation is reduced and the temporal variability is mostly driven by the production variability. The temporal variability of ^{10}Be deposition in this study is addressed in more detail in the accompanying paper (Heikkilä et al., 2013b).

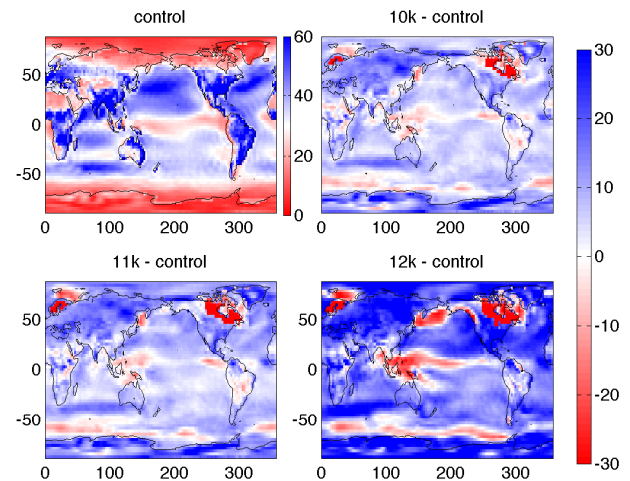


Fig. 9. Top left: sum of dry deposition and sedimentation in the control simulation ($\text{atoms m}^{-2} \text{s}^{-1}$). The remaining: Difference from control (%).

Due to the established connection between ^{10}Be and precipitation variability, it can be assumed that precipitation changes in a deglacial climate drive ^{10}Be deposition changes. The changes in ^{10}Be deposition partly follow the precipitation change, especially in the tropics (Figs. 4 and 7). Also, the positive change over Greenland and the negative one over Scandinavia and the Hudson Bay area are consistent with the precipitation change. However, the precipitation changes at 12k are larger than at 11k or 10k, which is not seen in the ^{10}Be deposition change, and the strongly negative precipitation change at 12k over North America does not correspond to the ^{10}Be deposition increase there. Table 1 shows that the global mean fraction of wet to total ^{10}Be deposition is similar in all simulations; however, it is reduced from the present-day value of 91–92% (Heikkilä et al., 2009). Figure 8 shows the spatial distribution of the change in wet fraction relative to ctrl. The change is small but roughly follows the precipitation change. In Scandinavia and the Hudson Bay area the wet fraction is increased (10%) instead of decreased, although the ^{10}Be deposition is decreased, suggesting a dilution effect. In Greenland, where the deposition change differs from the surrounding areas, no change is apparent in the wet fraction. In total the wet fraction change remains small (up to 15%), but locally the dry deposition and sedimentation increase by over 30% (Fig. 9). However, wet deposition remains the dominant method of removal of ^{10}Be from the atmosphere. To summarise, the ^{10}Be deposition differences globally are due to a combination of precipitation and atmospheric circulation changes, triggered by the increase in sea ice extent.

The circulation changes at mid- and high latitudes largely affect particle transport and dry deposition, which cause the air concentration of ^{10}Be to increase (Fig. 10). The largest increase in concentrations is found in the tropical tropopause

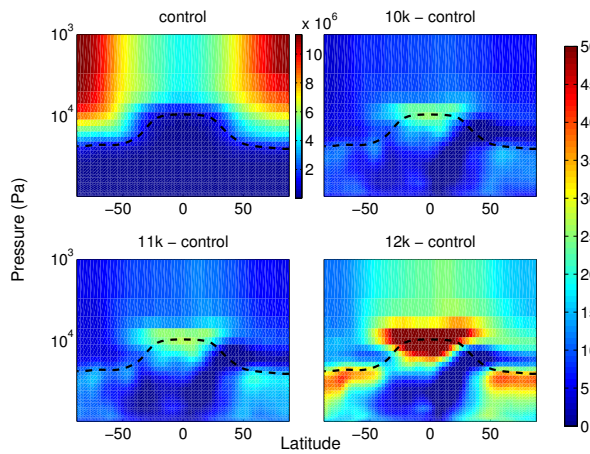


Fig. 10. Top left: zonal mean ¹⁰Be air concentration in the control simulation (atoms kg⁻¹). The remaining: Difference from control (%). The zonal mean tropopause height in the control simulation is indicated with the black dashed line.

region, indicating a weaker stratospheric transport. Outside of these regions there is a rather homogeneous increase of ca. 5 % in the 10k and 11k simulations. In the 12k simulation, however, the increase in the tropical tropopause region is much larger at up to 80 %, and a significant increase (ca. 40 %) is also apparent in the upper troposphere at high latitudes. The ¹⁰Be concentrations are also increased throughout the stratosphere. These changes follow the pattern of change of age of air between the simulations, derived from the modelled ¹⁰Be/⁷Be ratios (Fig. 11). ¹⁰Be and ⁷Be are produced in a near-constant ratio (gradually decreasing from 0.3 at ca. 30 km altitude to 0.8 near the surface (Heikkilä et al., 2008)) which increases because ⁷Be decays with its half-life of 53.2 days. The largely increased age of air in the stratosphere is consistent with the reduced strength of stratospheric zonal winds (Fig. 3). The differences are smallest at high latitudes where the production of new ¹⁰Be and ⁷Be decreases the mean ratio.

These changes in atmospheric circulation, ¹⁰Be air concentration and the transport path of ¹⁰Be from source to archive can potentially influence the mixture of ¹⁰Be from different atmospheric source regions in deposition. ¹⁰Be production varies by orders of magnitude across latitude and altitude. Furthermore, the production is more strongly modulated by varying solar activity at high latitudes and altitudes, where it is highest to begin with. Therefore, a change in the source-to-archive atmospheric transport path of ¹⁰Be could lead to a catchment of ¹⁰Be from a production area reflecting solar activity with a different amplitude from the global mean production. Figure 12 illustrates the source-to-archive distribution of ¹⁰Be for each of the simulations. The general distribution in these simulations is very similar to the previously studied present-day situations (Heikkilä and Smith, 2012, their Fig. 12): ¹⁰Be produced in the stratosphere is

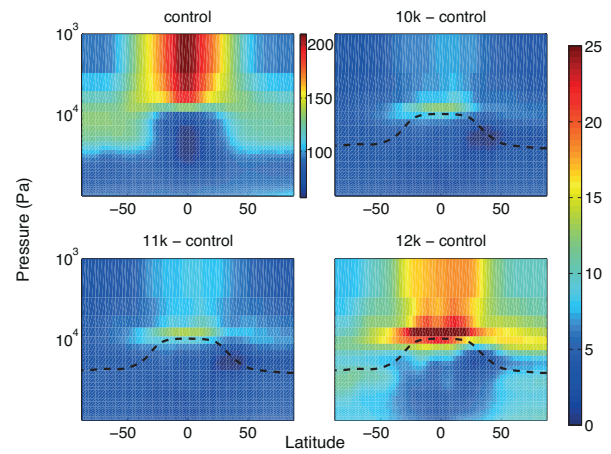


Fig. 11. Top left: zonal mean age of air derived from the ¹⁰Be/⁷Be in air in the control simulation (days). The remaining: difference from control (days). The zonal mean tropopause height in the control simulation is indicated with the black dashed line.

mainly transported into the troposphere via the mid-latitudes and deposited equally between the 0–30° and 30–60° latitude bands in each hemisphere. The tropospheric production of ¹⁰Be is mostly deposited locally, and the neighbouring latitude bands and rarely makes it to the opposite hemisphere. The figure shows that the differences between the control simulation and the deglaciation simulations are fairly small. In the SH the production and deposition distribution are practically unaffected by climatic changes in these simulations. The circulation change can be seen in latitude bands 30–60° N and 60–90° N, where the fraction of locally produced tropospheric ¹⁰Be in deposition is reduced by up to 8 % and exchanged within the next latitude band (more of the ¹⁰Be produced at 30–60° N is deposited at 60–90° N and vice versa). The reduced deposition and longer residence time allows for more longer-range transport within the troposphere. The stratospheric production of ¹⁰Be (ca. 2/3 of the total), which is also the most heavily modulated, is unaffected by the deglacial climate. The fairly large differences in atmospheric circulation found within the 10k, 11k and 12k simulations do not influence ¹⁰Be transport as much as between the control and any of the deglaciation simulations. These differences are comparable in amplitude with those caused by different model resolutions or realisations in Heikkilä and Smith (2012).

4 Summary and conclusions

This study investigates climatic influences on ¹⁰Be deposition during the last deglacial climate. Three time slice simulations were performed, each of 30 yr duration: 10 000 BP (10k), 11 000 BP (11k) and 12 000 BP (12k). These simulations were compared with a control (ctrl) simulation representing the preindustrial climate. The model employed was

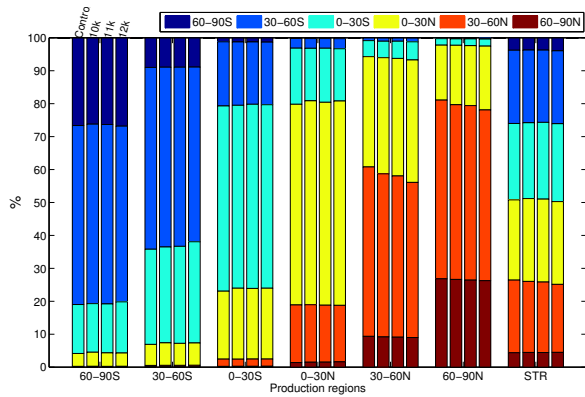


Fig. 12. Percentage of ^{10}Be , produced in a given atmospheric compartment (x axis, “STR” indicates the stratosphere), which is deposited at a given latitude band (legend) in the “ctrl”, “10k”, “11k” and “12k” simulations.

the atmospheric ECHAM5-HAM aerosol–climate model, driven by sea surface temperatures and sea ice cover produced by the coupled CSIRO Mk3L atmosphere–ocean–sea ice–land surface model. This paper, presenting the first part of this study, focuses on changes in atmospheric mean circulation and climate and their impact on the atmospheric distribution and deposition of ^{10}Be . The second part (Heikkilä et al., 2013b) investigates the influence of deglacial climate on ^{10}Be deposition in terms of preserving the solar signal. In order to separate the pure climate modulation of ^{10}Be , and also because the solar activity during the deglaciation is not known, ^{10}Be production was kept the same in all simulations. Hence the results are not suited for comparison with actual observations.

Generally the results follow changes in the GHGs. Surface temperatures are colder and the precipitation rate reduced in the 10k and 11k simulations from ctrl, and these differences are amplified in the 12k simulation. Similarly, stratospheric zonal winds are weakened in the 10k and 11k simulations, and more so in the 12k simulation. Moreover, there is a northward shift of westerly winds in the Northern Hemisphere upper troposphere. This decreases the precipitation change locally in Scandinavia and the Hudson Bay area, leading to a decreased ^{10}Be deposition in these areas, although the ^{10}Be deposition is generally decreased at mid- and high latitudes. Sea ice changes increase the fraction of wet deposition to total as opposed to the surrounding areas, where dry deposition is increased due to reduced precipitation rate. The reduced stratospheric winds lead to a reduced ^{10}Be transport, increasing the stratospheric residence time by 30 (10k and 11k) to 80 (12k) days. Tropospheric residence time is also increased by a few days, mainly at mid- to high latitudes due to the circulation changes. Atmospheric concentrations of ^{10}Be are strongly increased ($> 50\%$) in the upper troposphere at mid- to high latitudes and in the tropical tropopause region. These circulation changes seem to be attributed to the in-

crease in sea ice extent in the deglaciation simulations, leading to anomalies in geopotential height and shifts in the position of the polar jet. In the Southern Hemisphere (SH) the disturbances due to increased sea ice are only evident near the surface.

Despite the changes found in atmospheric circulation and the regionally varying response of ^{10}Be air concentrations, the source-to-archive distribution is fairly similar in all simulations. The largest change was found in the NH polar troposphere due to the reduced ^{10}Be deposition, leading to up to 8 % less deposition of locally produced ^{10}Be , compensated for by an increase of 0–30° N ^{10}Be . Most ^{10}Be produced in the stratosphere is deposited between 60° S and 60° N, uninfluenced by the deglacial climate. Generally the longer residence time in the deglaciation experiments allows for slightly increased long-range tropospheric transport in the NH. Due to the longer stratospheric residence time, the mixing of the large production gradients of ^{10}Be along latitude is more thorough.

These results indicate that ^{10}Be deposition is mostly determined by mass balance. If the production rate does not change, the global mean deposition change will be zero. Regionally the changes might be significant, but our results found only slight evidence for that. The increase in dry deposition by up to 50 % locally did not influence the spatial deposition variability much, because its total contribution remains small (12–13 % in all simulations). Varying climatic conditions and atmospheric circulation mainly affect the atmospheric residence time (80 days at most in these experiments), leading to a later deposition and a more thorough mixing of ^{10}Be . However, averaged over a few years, this effect is smoothed out. In fact, the longer residence time in colder climates leads to an increased mixing of ^{10}Be in the atmosphere and therefore a more homogeneous deposition pattern. Combining all these changes, the total deposition change was maximally 50 %. This is in agreement with the results of Alley et al. (1995), who found only moderate changes in ^{10}Be during the Younger Dryas.

Given these results, ^{10}Be deposition flux would be the optimal proxy for solar activity in an ideal archive because, following mass balance, the atmospheric production of ^{10}Be will have to be deposited at the surface within a few years. In case of ^{10}Be snow concentrations the mass balance does not necessarily hold due to potential changes in precipitation rate. In reality, however, the ^{10}Be deposition flux has to be derived from the reconstructed snow accumulation rate, which adds some uncertainty to the record. This uncertainty depends on each record and one has to refer to the original publications to quantify it.

Acknowledgements. This work was supported by an award under the Merit Allocation Scheme of the NCI National Facility at the ANU.

Edited by: V. Rath

References

- Alexander, M. A., Bhatt, U. S., Walsh, J. E., Timlin, M. S., Miller, J. S., and Scott, J. S.: The atmospheric response to realistic arctic sea ice anomalies in an AGCM during winter, *J. Climate*, 17, 890–905, 2004.
- Alley, R. B., Finkel, R. C., Nishiizumi, K., Anandkrishnan, S., Shuman, C. A., Mershon, G., Zielinski, G. A., and Mayewski, P. A.: Changes in continental and sea-salt atmospheric loadings in central Greenland during the most recent deglaciation: model-based estimates, *J. Glaciol.*, 41, 503–514, 1995.
- Blüthgen, J., Gerdes, R., and Werner, M.: Atmospheric response to the extreme Arctic sea ice conditions, *Geophys. Res. Lett.*, 39, L02707, doi:10.1029/2011GL050486, 2012.
- Bourgeois, Q. and Bey, I.: Pollution transport efficiency toward the Arctic: Sensitivity to aerosol scavenging and source regions, *J. Geophys. Res.*, 116, D08213, doi:10.1029/2010JD015096, 2011.
- Braconnot, P., Harrison, S. P., Kageyama, M., Bartlein, P. J., Masson-Delmotte, V., Abe-Ouchi, A., Otto-Bliesner, B., and Zhao, Y.: Evaluation of climate models using palaeoclimatic data, *Nat. Clim. Change*, 2, 417D424, doi:10.1038/nclimate1456, 2012.
- Budikova, D.: Role of Arctic sea ice in global atmospheric circulation: A review, *Global Planet. Change*, 68, 149–163, doi:10.1016/j.gloplacha.2009.04.001, 2009.
- Heikkilä, U., Beer, J., and Alifimov, V. A.: Beryllium-10 and beryllium-7 in precipitation in Dübendorf (440 m) and at Jungfraujoch (3580 m), Switzerland (1998–2005), *J. Geophys. Res.*, 113, D11104, doi:10.1029/2007JD009160, 2008.
- Heikkilä, U., Beer, J., and Feichter, J.: Meridional transport and deposition of atmospheric ¹⁰Be, *Atmos. Chem. Phys.*, 9, 515–527, doi:10.5194/acp-9-515-2009, 2009.
- Heikkilä, U. and Smith, A. M.: Influence of model resolution on the atmospheric transport of ¹⁰Be, *Atmos. Chem. Phys.*, 12, 10601–10612, doi:10.5194/acp-12-10601-2012, 2012.
- Heikkilä, U. and Smith, A. M.: Production rate and climate influences on the variability of ¹⁰Be deposition simulated by ECHAM5-HAM: Globally, in Greenland, and in Antarctica, *J. Geophys. Res. Atmos.*, 118, 2506–2520, doi:10.1002/jgrd.50217, 2013a.
- Heikkilä, U., Shi, X., Phipps, S. J., and Smith, A. M.: ¹⁰Be in late deglacial climate simulated by ECHAM5-HAM – Part 2: Isolating the solar signal from ¹⁰Be deposition, *Clim. Past Discuss.*, 9, 5627–5657, doi:10.5194/cpd-9-5627-2013, 2013.
- Koch, D., Schmidt, G. A., and Field, C. V.: Sulfur, sea salt and radionuclide aerosols in GISS ModelE, *J. Geophys. Res.*, 111, D06206, doi:10.1029/2004JD005550, 2006.
- Krinner, G., Petit, J.-R., and Delmonte, B.: Altitude of atmospheric tracer transport towards Antarctica in present and glacial climate, *Quaternary Sci. Rev.*, 29, 274–284, doi:10.1016/j.quascirev.2009.06.020, 2010.
- Land, C. and Feichter, J.: Stratosphere-troposphere exchange in a changing climate simulated with the general circulation model MAECHAM4, *J. Geophys. Res.*, 108, 8523, doi:10.1029/2002JD002543, 2003.
- Liu, Z., Otto-Bliesner, B. L., He, F., Brady, E. C., Tomas, R., Clark, P. U., Carlson, A. E., Lynch-Stieglitz, J., Curry, W., Brook, E., Erickson, D., Jacob, R., Kutzbach, J., and Cheng, J.: Transient simulation of the last deglaciation with a new mechanism for Bølling-Allerød warming, *Science*, 325, 310–314, doi:10.1126/science.1171041, 2009.
- Mahowald, N. M., Muhs, D. R., Lewis, S., Rasch, P. J., Yoshioka, M., Zender, C. S., and Luo, C.: Change in atmospheric mineral mineral aerosols in response to climate: last glacial period, preindustrial, modern, and doubled carbon dioxide climates, *J. Geophys. Res.*, 111, D10202, doi:10.1029/2005JD006653, 2006.
- Muscheler, R., Beer, J., Wagner, G., and Finkel, R. C.: Changes in deep-water formation during the Younger Dryas event inferred from ¹⁰Be and ¹⁴C, *Nature*, 408, 567–570, 2000.
- Muscheler, R., Beer, J., Wagner, G., Laj, C., Kissel, C., Raisbeck, G. M., Yiou, F., and Kubik, P. W.: Changes in the carbon cycle during the last deglaciation as indicated by the comparison of ¹⁰Be and ¹⁴C/records, *EPSL*, 6973, 1–16, doi:10.1016/S0012-821X(03)00722-2, 2004.
- Overland, J. E. and Wang, M.: Large-scale atmospheric circulation changes are associated with the recent loss of Arctic sea ice, *Tellus*, 62A, 1–9, doi:10.1111/j.1600-0870.2009.00421.x, 2010.
- Peltier, W. R.: Global Glacial Isostasy and the Surface of the Ice-Age Earth: The ICE-5G (VM2) Model and GRACE, *Ann. Rev. Earth Planet. Sci.*, 32, 111–149, 2004.
- Phipps, S. J., Rotstayn, L. D., Gordon, H. B., Roberts, J. L., Hirst, A. C., and Budd, W. F.: The CSIRO Mk3L climate system model version 1.0 – Part 1: Description and evaluation, *Geosci. Model Dev.*, 4, 483–509, doi:10.5194/gmd-4-483-2011, 2011.
- Phipps, S. J., Rotstayn, L. D., Gordon, H. B., Roberts, J. L., Hirst, A. C., and Budd, W. F.: The CSIRO Mk3L climate system model version 1.0 – Part 2: Response to external forcings, *Geosci. Model Dev.*, 5, 649–682, doi:10.5194/gmd-5-649-2012, 2012.
- Roth, R. and Joos, F.: A reconstruction of radiocarbon production and total solar irradiance from the Holocene ¹⁴C and CO₂ records: implications of data and model uncertainties, *Clim. Past*, 9, 1879–1909, doi:10.5194/cp-9-1879-2013, 2013.
- Screen, J. A. and Simmonds, I.: The central role of diminishing sea ice in recent Arctic temperature amplification, *Nature*, 464, 1334–1337, doi:10.1038/nature09051, 2010.
- Shakun, J. D. and Carlson, A. E.: A global perspective on Last Glacial Maximum to Holocene climate change, *Quaternary Sci. Rev.*, 29, 1801–1816, doi:10.1016/j.quascirev.2010.03.016, 2010.
- Steinhilber, F., Abreu, J. A., Beer, J., Brunner, I., Christl, M., Fischer, H., Heikkilä, U., Kubik, P. W., Mann, M., McCracken, K. G., Miller, H., Miyahara, H., Oerter, H., and Wilhelms, F.: 9,400 years of cosmic radiation and solar activity from ice cores and tree rings, *Proc. Natl. Acad. Sci.*, 109, 5967–5971, doi:10.1073/pnas.1118965109, 2012.
- Trenberth, K. E., Jones, P. D., Ambenje, P., Bojariu, R., Easterling, D., Tank, A. K., Parker, D., Rahimzadeh, F., Renwick, J. A., Rusticucci, M., Soden, B., and Zhai, P.: Observations: surface and atmospheric climate change, in: *Climate Change 2007: The Physical Science Basis*, edited by: Solomon, S., Qin, D., Manning, M., Chen, Z., Marquis, M., Averyt, K. B., Tignor, M., and Miller, H. L., Chap. 3, Cambridge University Press, Cambridge, 235D336, 2007.